Mathematical and Computational Applications

MDPI

Article

Eigenstructure-Oriented Optimization Design of Active Suspension Controllers

Yulong Du and Huping Mao *

School of Energy and Power Engineering, North University of China, Taiyuan 030051, China; yulongdu2023@163.com
* Correspondence: maohp@nuc.edu.cn; Tel.: +86-18035395956

Abstract

Active suspension systems can significantly enhance vehicle ride comfort and attitude stability, but often at the cost of increased energy consumption. To achieve both high dynamic performance and reduced energy usage, this study proposes an eigenstructure-oriented optimization method for active suspensions. Controller design is reformulated as a synergistic process of modal regulation and dynamic response optimization, in which partial eigenstructure assignment redistributes the dominant modes and system responses are computed using fourth-order Runge–Kutta integration. An energy-minimization optimization problem with performance constraints is then solved via the sequential quadratic programming (SQP) algorithm. Simulation results show that the proposed method markedly improves vibration performance: peak body acceleration is reduced from 3.48 m/s^2 to 1.70 m/s^2 (a 51.1% reduction), and the root mean square (RMS) acceleration decreases from 0.74 to 0.40 (a 45.6% reduction), while body displacement is also significantly suppressed. Compared with passive suspension and proportional–integral–derivative (PID) active suspension, the proposed system achieves superior performance in key indices such as body acceleration and displacement, leading to noticeably improved ride comfort and attitude stability. Furthermore, robustness analysis indicates that the method remains effective under variations in the receptance matrix, with only minor influence on system performance, demonstrating the practical applicability of the proposed control strategy.

Keywords: eigenstructure assignment; active suspension; dynamic response optimization; controller design

Check for updates

Academic Editor: Guillermo Valencia-Palomo

Received: 5 November 2025
Revised: 19 December 2025
Accepted: 19 December 2025
Published: 1 January 2026

Copyright: © 2026 by the authors. Licensee MDPI, Basel, Switzerland. This article is an open access article distributed under the terms and conditions of the Creative Commons Attribution (CC BY) license.

1. Introduction

With the continuous development of the automotive industry and the rising demand for driving safety and ride comfort, suspension performance optimization has become a central topic in vehicle dynamics. During operation, uneven road surfaces and external disturbances excite significant vibrations of the vehicle body and associated components. These vibrations not only degrade ride comfort and handling stability but also accelerate component wear and may even compromise driving safety. Consequently, vibration suppression and accurate control of body motion have become key objectives in suspension system design.

Traditionally, passive suspension systems have been widely used because of their simple structure and low cost. Such systems rely on fixed-parameter elements, including springs and dampers, to passively respond to road excitations. Although they provide basic vibration isolation under normal conditions, their fixed parameters prevent real-time

adaptation to varying road surfaces. As a result, their performance under complex or extreme driving conditions is limited, making it difficult to simultaneously satisfy the requirements of ride comfort and handling stability in modern vehicles.

To overcome these limitations, active suspension systems have been extensively investigated. By employing actuators to actively generate control forces, they can dynamically adjust suspension stiffness and damping, thereby enabling real-time control of vehicle body motion. Compared with passive suspensions, active systems offer markedly improved ride comfort and handling stability, as well as superior adaptability to changing operating environments. However, their complex structure imposes stringent requirements on control strategy design—particularly in terms of real-time performance, stability and energy efficiency—which has driven ongoing research into advanced control methodologies.

Active suspension control has evolved rapidly over the past decade, driven by the need to improve both ride comfort and vehicle stability. Many studies focus on refining classical optimal and robust control strategies. Recent work has enhanced linear quadratic regulator (LQR) schemes through advanced optimization techniques [1–7], improved tracking and robustness via fuzzy logic and sliding-mode controllers [5,8–13], and strengthened disturbance rejection using H-infinity (H∞) and adaptive fault-tolerant control [9–11]. Although these methods deliver notable performance gains, they are largely incremental extensions of traditional model-based control paradigms. Their emphasis lies mainly on algorithmic tuning or controller restructuring, rather than on fundamentally reshaping the dynamic behavior of the suspension. As a result, the reported improvements, while effective, are predominantly performance-driven yet largely agnostic to the system's eigenstructure.

A parallel line of research has introduced increasingly sophisticated nonlinear, intelligent and learning-based strategies. Adaptive fuzzy control, fractional-order control, and inverse optimal control have expanded the capacity to address system uncertainties and nonlinearities [14–17]. Model predictive control (MPC) has been adapted to handle speed-dependent dynamics and preview information [18,19], while hybrid metaheuristic–fuzzy schemes have shown potential for enhanced global optimization [20]. More recently, neural-network-based adaptive control and deep reinforcement learning (DRL) have achieved impressive response improvements and generalization capabilities under complex operating conditions [21–25]. Despite these advances, most intelligent and learning-based approaches continue to treat the suspension as an input–output mapping to be optimized, rather than as a dynamical structure whose underlying eigenproperties fundamentally determine system performance. Consequently, these methods often require extensive training data, rely on heuristic reward or parameter tuning, and offer limited physical interpretability.

Complementary to these control-centric approaches, structural dynamics research has highlighted the importance of eigenvalues and eigenvectors as intrinsic determinants of system behavior. A series of studies has advanced eigenstructure assignment techniques, including model updating [26], concurrent parameter and controller optimization [27], partial pole or pole–zero placement [28–30], time-delay compensation [31], and receptance-based assignment using partial data [32,33]. These works significantly reduce reliance on accurate system matrices and deepen theoretical understanding of structural feature manipulation. However, their impact remains largely confined to the vibration control and structural modification communities. The application of eigenstructure assignment to active suspension control has been surprisingly limited. Most existing studies provide conceptual formulations or simulation demonstrations but lack systematic pathways for embedding eigenstructure manipulation into practical control design.

Overall, the literature reveals a clear gap. On the one hand, control-oriented studies primarily enhance controller performance but seldom exploit the intrinsic structural characteristics that fundamentally shape suspension dynamics. On the other hand, research

on structural feature regulation mainly addresses theoretical formulations and vibration-oriented applications, with limited integration into practical suspension control, especially when performance constraints and energy consumption are considered simultaneously. To bridge this gap, the present study a standard quarter-car active suspension model and proposes an eigenstructure-oriented optimization design method. By combining partial eigenstructure assignment with dynamic-response-based optimization, the method improves suspension performance while explicitly limiting controller gain magnitude and energy consumption

The main contributions of this study are as follows:

1. An eigenstructure-oriented optimization framework is developed for active suspension systems. This framework provides a physically interpretable means of regulating structural dynamics and enables targeted modal control to enhance vibration isolation performance.
2. A performance-constrained optimization strategy is established to enhance suspension performance while limiting control effort, ensuring that ride comfort enhancement is achieved in parallel with reduced gain magnitude and energy consumption.

The remainder of this paper is organized as follows. Section 2 introduces the quarter-car active suspension model and the corresponding road-excitation representation. Section 3 presents the proposed eigenstructure-oriented controller design and the associated optimization formulation, including implementation details. Section 4 reports numerical studies and discussions based on a representative parameter set. Section 5 investigates the robustness of the resulting controller. Section 6 concludes the paper and outlines the limitations and directions for future work.

2. System Modeling

2.1. Mathematical Modeling of Active Suspension

To analyze the vertical dynamic response of a vehicle subjected to road excitation, this study adopts a classical quarter-car active suspension model with two degrees of freedom (2-DoF), as illustrated in Figure 1.

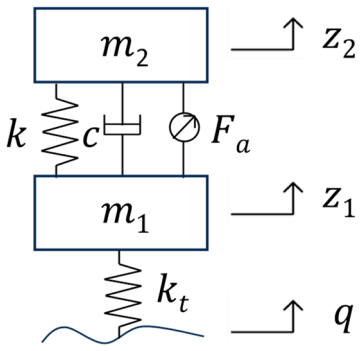


Figure 1. Schematic diagram of the quarter-car active suspension system.

In this model, the actuator is modeled as an ideal force source, and the suspension spring and damper are assumed to be linear elements. Nonlinear effects, frictional losses and structural coupling are neglected so that a linear system suitable for analysis and controller design is obtained.

In the model, m_2 denotes the sprung mass, approximately one quarter of the total vehicle mass, and m_1 denotes the unsprung mass, mainly comprising the wheel and its associated components. F_a is the control force acting between the sprung and unsprung masses to actively regulate the dynamic response. k and c are the equivalent suspension stiffness and damping, respectively, and k_t represents the tire stiffness. z_2 and z_1 represent

the vertical displacements of the sprung and unsprung masses, respectively, and q is the road excitation input.

Accordingly, the vertical motions of the unsprung and sprung masses are governed by Equations (1) and (2), respectively, and can be expressed as follows:

The unsprung mass:

$$m_1\ddot{z}_1 + k_t(z_1 - q) - c(\dot{z}_2 - \dot{z}_1) - k(z_2 - z_1) = -F_a \tag{1}$$

The sprung mass:

$$m_2\ddot{z}_2 + c(\dot{z}_2 - \dot{z}_1) + k(z_2 - z_1) = F_a \tag{2}$$

2.2. Road Excitation Modeling

In the analysis and design of vehicle suspension dynamics, accurately representing external road excitation is essential. During driving, road surface irregularities are transmitted through the tire to the suspension system and constitute the primary external disturbance affecting overall ride and handling performance. A widely adopted modeling approach is to describe the road profile using the Power Spectral Density (PSD) function proposed by the International Organization for Standardization (ISO 8608, [34]).

In general, road surface irregularities can be modeled as a broadband random process whose spatial power spectral density is given by Equation (3):

$$G_q(n) = G_q(n_0)\left(\frac{n}{n_0}\right)^{-\omega} \tag{3}$$

where $G_q(n_0)$ is the road roughness coefficient at the reference spatial frequency n_0; n denotes the spatial frequency; ω is the frequency exponent, which is usually taken as 2. Different road classes correspond to different values of $G_q(n_0)$, as summarized in Table 1.

Table 1. Classification of road surface roughness.

Road Surface Class	Roughness Coefficient $G_q(n_0)$ ($\times 10^{-6}$ m^3)
A	16
B	64
C	256
D	1024
E	4096
F	16,384

Road excitation depends not only on surface roughness but also on vehicle speed, both of which are key factors influencing the dynamic behavior of suspension systems. To achieve realistic time-domain simulations, the spatial power spectral density must be correlated with vehicle speed v and transformed into the temporal frequency domain. The spatial frequency n and temporal frequency f are related by Equation (4):

$$f = nv \tag{4}$$

Accordingly, the spatial power spectral density can be converted into the frequency domain, and the corresponding expression is given by Equation (5):

$$G_q(n) = G_q(n_0)\left(\frac{n_0}{f/v}\right)^2 v \tag{5}$$

where f denotes the temporal frequency and v is the vehicle speed.

Introducing the angular frequency $\omega = 2\pi f$, the corresponding expression of the road excitation in the frequency domain can be rewritten as Equation (6):

$$G_q(\omega) = \frac{4\pi^2 G_q(n_0) n_0^2 v}{\omega^2 + \omega_0^2} \tag{6}$$

where $\omega_0 = 2\pi n_0 v$ represents the lower cutoff angular frequency, and n_0 is the lower cutoff spatial frequency.

The time-domain representation of the road excitation can be generated through a first-order filtering process driven by white noise, as given in Equation (7):

$$\dot{q}(t) = -2\pi n_1 q(t) + 2\pi\omega(t) n_0 \sqrt{G_q(n_0) v} \tag{7}$$

where $\omega(t)$ denotes unit-intensity Gaussian white noise.

3. Theory and Methodology

3.1. Theory of Eigenstructure Assignment

For an n-DoF linear time-invariant system, the open-loop dynamic equation can be expressed as Equation (8):

$$\mathbf{M}\ddot{\boldsymbol{x}}(t) + \mathbf{C}\dot{\boldsymbol{x}}(t) + \mathbf{K}\boldsymbol{x}(t) = 0 \tag{8}$$

where $\boldsymbol{x}(t) \in \mathbb{R}^n$ is the vector of generalized coordinates, and $\mathbf{M}, \mathbf{C}, \mathbf{K} \in \mathbb{R}^{n\times n}$ denote the mass, damping, and stiffness matrices, respectively.

When an active control force $\boldsymbol{u}(t)$ is introduced, the closed-loop dynamic equation is given by Equation (9):

$$\mathbf{M}\ddot{\boldsymbol{x}}(t) + \mathbf{C}\dot{\boldsymbol{x}}(t) + \mathbf{K}\boldsymbol{x}(t) = \mathbf{B}\boldsymbol{u}(t) \tag{9}$$

where $\mathbf{B} \in \mathbb{R}^{n\times p}$ is the control input distribution matrix and $\boldsymbol{u}(t) \in \mathbb{R}^p$ is the control input vector. The control law is defined as $\boldsymbol{u}(t) = -\mathbf{F}^T\dot{\boldsymbol{x}}(t) - \mathbf{G}^T\boldsymbol{x}(t)$, where $\mathbf{F}, \mathbf{G} \in \mathbb{R}^{n\times p}$ represent the feedback gain matrices corresponding to velocity and displacement, respectively.

The quadratic eigenvalue problems of the open-loop and closed-loop systems are formulated in Equations (10) and (11):

$$\left(\lambda_k^2\mathbf{M} + \lambda_k\mathbf{C} + \mathbf{K}\right)\boldsymbol{v}_k = 0 \tag{10}$$

$$\left(\mu_k^2\mathbf{M} + \mu_k\mathbf{C} + \mathbf{K}\right)\boldsymbol{w}_k = \mathbf{B}\left(\mathbf{G}^{\mathrm{T}} + \mu_k\mathbf{F}^{\mathrm{T}}\right)\boldsymbol{w}_k \tag{11}$$

where $(\lambda_i, \mathbf{v}_i)$ and $(\mu_k, \mathbf{w}_k)$ are the eigenpairs of the open-loop and closed-loop systems, respectively.

Equation (11) can be rearranged into the homogeneous form shown in Equation (12):

$$\left(\mu_k^2\mathbf{M} + \mu_k\mathbf{C} + \mathbf{K} - \mathbf{B}\left(\mathbf{G}^{\mathrm{T}} + \mu_k\mathbf{F}^{\mathrm{T}}\right)\right)\boldsymbol{w}_k = \mathbf{0} \tag{12}$$

Assuming that the first $2p$ closed-loop eigenvalues are reassigned, while the $2p+1, \cdots, 2n$ eigenvalues remain unchanged, we impose the following condition (Equation (13)):

$$\lambda_k = \mu_k, \qquad k = 2p+1, \cdots, 2n \tag{13}$$

Introducing an auxiliary mass modification matrix $\Delta\mathbf{M}$ (used only for analytical derivation and not implemented in practice), Equation (12) can be rewritten as Equation (14):

$$\left(\lambda_k^2(\mathbf{M} + \boldsymbol{\Delta}\mathbf{M}) + \lambda_k\mathbf{C} + \mathbf{K}\right)\boldsymbol{w}_k = \mathbf{B}\left(\mathbf{G}^{\mathrm{T}} + \lambda_k\mathbf{F}^{\mathrm{T}}\right)\boldsymbol{w}_k + \lambda_k^2\boldsymbol{\Delta}\mathbf{M}\boldsymbol{w}_k \tag{14}$$

https://doi.org/10.3390/mca31010005

where $k = 2p+1, \cdots, 2n$.

Defining $\hat{\mathbf{H}}(\mu_k) = \left(\lambda_k^2(\mathbf{M}+\mathbf{\Delta M}) + \lambda_k \mathbf{C} + \mathbf{K}\right)^{-1}$, and pre-multiplying both sides of Equation (14) by $\hat{\mathbf{H}}(\mu_k)$, we obtain Equation (15):

$$\boldsymbol{w}_k = \hat{\mathbf{H}}(\mu_k)\mathbf{B}\left(\mathbf{G}^{\mathrm{T}} + \lambda_k \mathbf{F}^{\mathrm{T}}\right)\boldsymbol{w}_k + \lambda_k^2 \hat{\mathbf{H}}(\mu_k)\mathbf{\Delta M}\boldsymbol{w}_k, \qquad k = 2p+1, \cdots, 2n \tag{15}$$

Rearranging Equation (15) yields Equation (16):

$$\left(\mathbf{I} - \lambda_k^2 \hat{\mathbf{H}}(\mu_k)\mathbf{\Delta M}\right)\boldsymbol{w}_k = \hat{\mathbf{H}}(\mu_k)\mathbf{B}\left(\mathbf{G}^{\mathrm{T}} + \lambda_k \mathbf{F}^{\mathrm{T}}\right)\boldsymbol{w}_k, \qquad k = 2p+1, \cdots, 2n \tag{16}$$

Finally, Equation (16) can be reformulated in the compact form of Equation (17):

$$\left(\mathbf{I} - \lambda_k^2 \hat{\mathbf{H}}(\mu_k)\mathbf{\Delta M}\right)\boldsymbol{w}_k = \boldsymbol{u}_k, \qquad k = 2p+1, \cdots, 2n \tag{17}$$

To facilitate subsequent derivations, a proportional coefficient vector is introduced as $\boldsymbol{\beta}_k = \begin{bmatrix}\beta_{k1} & \beta_{k2} & \cdots & \beta_{ki}\end{bmatrix}^T$ and defined in Equation (18):

$$\beta_{kj} = \left(\mu_k \boldsymbol{f}_j^T + \boldsymbol{g}_j^T\right)\boldsymbol{w}_k, \qquad j = 1, 2, \cdots, i \tag{18}$$

It is noteworthy that the modal vectors $\mathbf{w}_k$ are assumed to be predetermined.

By substituting Equation (18) into Equation (17), the compact expression in Equation (19) is obtained for the eigenvalues kept unchanged:

$$\boldsymbol{u}_k = \hat{\mathbf{H}}(\mu_k)\mathbf{B}\boldsymbol{\beta}_k, \qquad k = 2p+1, \cdots, 2n \tag{19}$$

Similarly, by defining $\mathbf{H}(\mu_k) = \left(\lambda_k^2 \mathbf{M} + \lambda_k \mathbf{C} + \mathbf{K}\right)^{-1}$ and referring to Equation (12), the corresponding relation for the reassigned eigenvalues can be written as Equation (20):

$$\boldsymbol{w}_k = \mathbf{H}(\mu_k)\mathbf{B}\boldsymbol{\beta}_k, \qquad k = 1, \cdots, 2p \tag{20}$$

Equations (19) and (20) can thus be unified in the form of Equation (21):

$$\mathbf{B}\boldsymbol{\beta}_k = \boldsymbol{\gamma}_k \tag{21}$$

where $\boldsymbol{\gamma}_k$ is defined piecewise in Equation (22):

$$\boldsymbol{\gamma}_k = \begin{cases} \mathbf{H}(\mu_k)^{-1}\boldsymbol{w}_k, & k = 1, \cdots, 2p \\ \hat{\mathbf{H}}(\mu_k)^{-1}\boldsymbol{u}_k, & k = 2p+1, \cdots, 2n \end{cases} \tag{22}$$

From Equation (22), the proportional coefficient vector $\boldsymbol{\beta}_k$ can be subsequently obtained.

Using the definition in Equation (18), this relationship can be written in matrix form as Equation (23):

$$\begin{bmatrix} \mu_k \boldsymbol{w}_k^T & 0 & \cdots & 0 & \boldsymbol{w}_k^T & 0 & \cdots & 0 \\ 0 & \mu_k \boldsymbol{w}_k^T & \cdots & 0 & 0 & \boldsymbol{w}_k^T & \cdots & 0 \\ \vdots & \vdots & \vdots & \vdots & \vdots & \vdots & \vdots & \vdots \\ 0 & 0 & \cdots & \mu_k \boldsymbol{w}_k^T & 0 & 0 & \cdots & \boldsymbol{w}_k^T \end{bmatrix} \begin{bmatrix} \boldsymbol{f}_1 \\ \vdots \\ \boldsymbol{f}_i \\ \boldsymbol{g}_1 \\ \vdots \\ \boldsymbol{g}_i \end{bmatrix} = \begin{bmatrix} \beta_{k1} \\ \beta_{k2} \\ \vdots \\ \beta_{ki} \end{bmatrix}, \; k = 1, \cdots, 2n \tag{23}$$

Accordingly,

$$\mathbf{T}_k \boldsymbol{y} = \boldsymbol{\beta}_k, \qquad k = 1, 2, \cdots, 2n \tag{24}$$

Consequently, the gain matrices **G** and **F** of the controller can be determined from the global matrix equation in Equation (25):

$$\begin{bmatrix} \mathbf{T}_1 \\ \vdots \\ \mathbf{T}_{2n} \end{bmatrix} \begin{bmatrix} f_1 \\ \vdots \\ f_i \\ g_1 \\ \vdots \\ g_i \end{bmatrix} = \begin{bmatrix} \boldsymbol{\beta}_1 \\ \vdots \\ \boldsymbol{\beta}_{2n} \end{bmatrix} \tag{25}$$

3.2. Dynamic Response Optimization Approach

In the optimization design of the active suspension system, the RMS values of the body acceleration and displacement are adopted as the primary performance indices, while the minimization of the controller gains is defined as the optimization objective. This formulation aims to enhance suspension performance while simultaneously maintaining energy efficiency. To obtain the desired system response over a finite time interval $[0, t_{\text{end}}]$, the design variables are optimized under engineering constraints and within prescribed bounds.

For the two-degree-of-freedom (2-DoF) quarter-car active suspension model, the predefined modal vectors $\mathbf{w}_k$ (assembled in $\mathbf{X} = [\mathbf{v}_1^{\mathrm{T}}, \mathbf{v}_2^{\mathrm{T}}, \cdots, \mathbf{v}_n^{\mathrm{T}}]^{\mathrm{T}}$) and the system eigenvalues λ_k (collected in $Y = \lambda_k$) are chosen as the design variables. Based on the system dynamic equations and the eigenstructure assignment theory, a mathematical model for dynamic response optimization of the active suspension system is then established.

$$min \sum_{i=1}^{n} \sum_{j=1}^{m} \left(f(\boldsymbol{X}, Y, \mu_c)_{ij}^2 + g(\boldsymbol{X}, Y, \mu_c)_{ij}^2 \right)$$

$$s.t. \begin{cases} T \begin{bmatrix} f_1 & \cdots & f_m & g_1 & \cdots & g_m \end{bmatrix}^T = \begin{bmatrix} \boldsymbol{\beta}_1 \\ \vdots \\ \boldsymbol{\beta}_{2n} \end{bmatrix} \\ \left(\mathbf{Y}^2 \mathbf{M} + \mathbf{Y}(\mathbf{C} + \mathbf{B}\mathbf{F}^{\mathrm{T}}) + \left(\mathbf{K} - \mathbf{B}\mathbf{G}^{\mathrm{T}} \right) \right) \boldsymbol{w}_k = 0 \\ \mathbf{M}\ddot{d}_p(t) + (\mathbf{C} - \mathbf{B}\mathbf{F}^{\boldsymbol{T}})\dot{d}_p(t) + \left(\mathbf{K} - \mathbf{B}\mathbf{G}^{\boldsymbol{T}} \right) d_p(t) = f_r(t) \\ \left[\frac{1}{T} \int_0^T d_{pw}^2(t) dt \right]^{\frac{1}{2}} \leq c_1, \quad p = 1, 2, \cdots, ug \\ \left[\frac{1}{T} \int_0^T \ddot{d}_{pw}^2(t) dt \right]^{\frac{1}{2}} \leq c_2, \quad p = 1, 2, \cdots, ug \\ \mathbf{X}_{min} \leq \mathbf{X} \leq \mathbf{X}_{max} \\ Y_{min} \leq Y \leq Y_{max} \end{cases} \tag{26}$$

$$i = 1, 2, \cdots, n;\ j = 1, 2, \cdots, m; c = 2p + 1, \cdots, 2n$$

In this model, c_1 and c_2 denote the RMS performance indices of body displacement and body acceleration, respectively; d_p and $\ddot{d}_p$ represent the displacement and acceleration responses at the p-th coordinate ($p = 2$ for the vehicle body); and the design variables **X** and Y are constrained within $[\mathbf{X}_{\min}, \mathbf{X}_{\max}]$ and $[Y_{\min}, Y_{\max}]$, respectively.

To clarify the implementation procedure of the proposed method, the overall optimization framework is summarized in Figure 2 and can be outlined as follows:

(1) Define the eigenvalues to be reassigned and those to be retained;

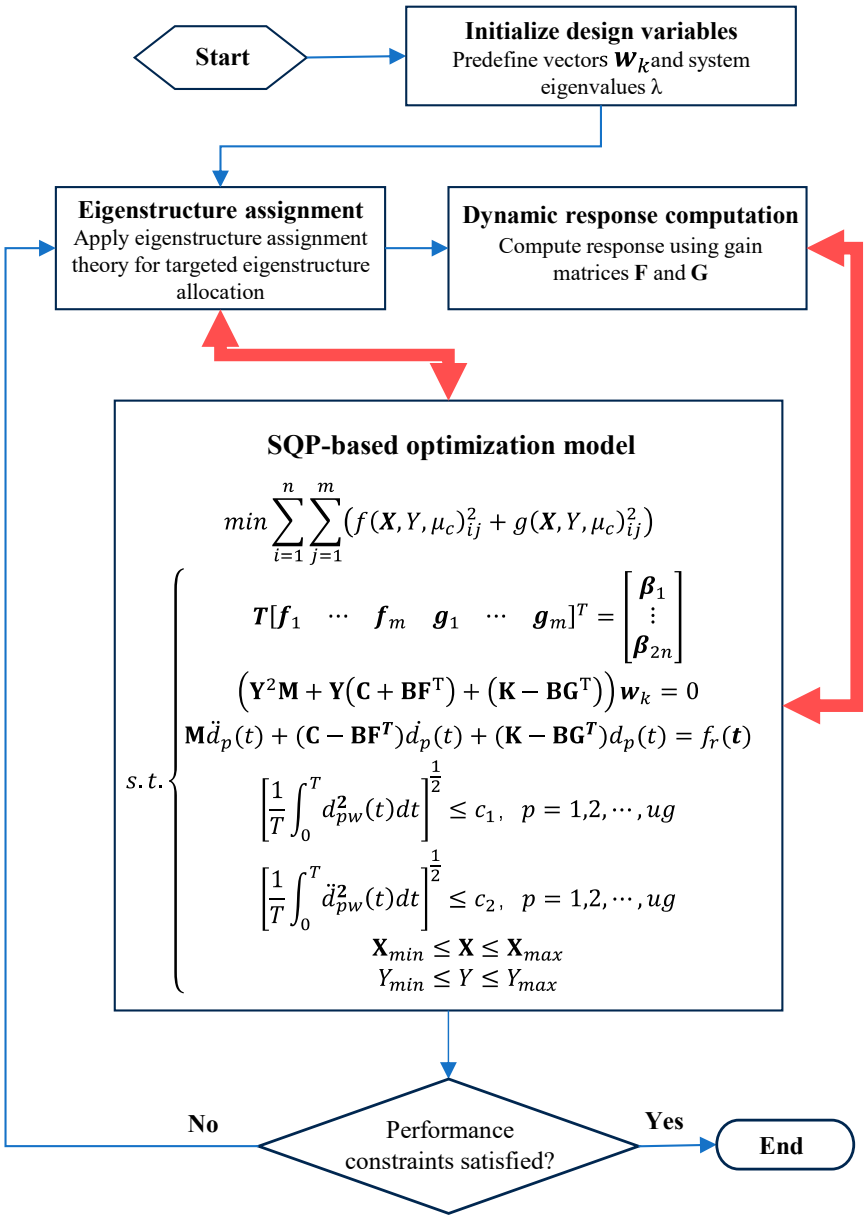


Figure 2. Flowchart of dynamic response optimization.

(2) Select the design variables (the predefined vectors $\mathbf{w}_k$ and the system eigenvalues λ_k) together with the performance indices, and establish the corresponding mathematical optimization model;
(3) Assign initial values to the design variables and compute the initial controller gain matrices using the partial eigenstructure assignment method;
(4) Substitute the gain matrices into the system dynamic equations and perform a time-domain response analysis using the fourth-order Runge–Kutta method;
(5) Iteratively update the design variables using the SQP algorithm until convergence to the optimal solution.

4. Numerical Example

The parameters used for the quarter-car suspension model are listed in Table 2.

Table 2. Suspension system parameters.

Parameter	Symbol	Value	Unit
Sprung mass	m_2	317	kg
Unsprung mass	m_1	45	kg
Suspension stiffness	k	22,000	N/m
Suspension damping coefficient	c	1500	Ns/m
Tire stiffness	k_t	192,000	N/m

Based on the above parameters, the system matrices of the quarter-car model can be expressed as follows:

$$\mathbf{M} = \begin{bmatrix} 317 & 0 \\ 0 & 45 \end{bmatrix}, \mathbf{K} = \begin{bmatrix} 22000 & -22000 \\ -22000 & 214000 \end{bmatrix}, \mathbf{C} = \begin{bmatrix} 1500 & -1500 \\ -1500 & 1500 \end{bmatrix}$$

The open-loop system possesses two pairs of complex conjugate eigenvalues:

$$\lambda_{1,2} = -17.0876 \pm 65.8487i, \lambda_{3,4} = -1.9450 \pm 7.7588i$$

The corresponding eigenvectors are also obtained, as summarized in Table 3.

Table 3. Eigenvalues and corresponding eigenvectors of the open-loop system.

λ_k	$\mathbf{v}_k^T$	
$-17.0876 + 65.8487i$	$0.0281 + 0.0632$i	$-0.9976 + 0.0095i$
$-17.0876 - 65.8487$i	$0.0281 - 0.0632$i	$-0.9976 - 0.0095i$
$-1.9450 + 7.7588i$	$0.2391 - 0.9651i$	$0.0719 - 0.0785i$
$-1.9450 - 7.7588i$	$0.2391 + 0.9651i$	$0.0719 + 0.0785i$

To obtain the dynamic response of the suspension system under open-loop conditions, a typical ISO Class C random road profile was selected as the external excitation. The road roughness parameters were set as follows: $G_q(n_0) = 256 \times 10^{-6}$ m^3, $v = 72$ km/h, $t = 10$ s, with the random noise seed set to 233. The typical Class C road profile excitation signal is illustrated in Figure 3.

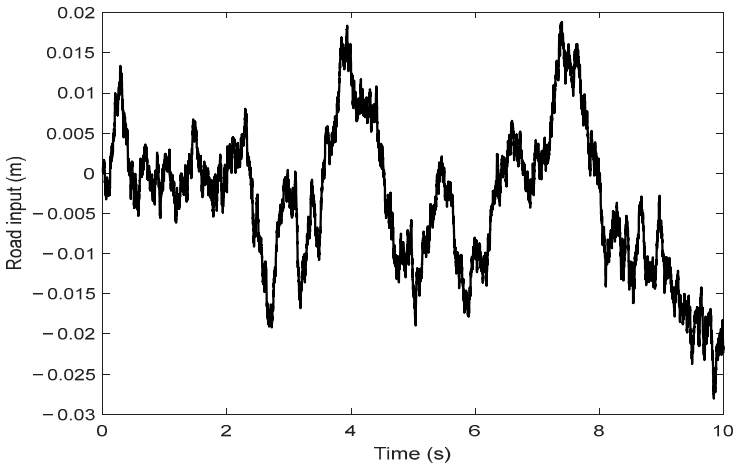


Figure 3. Road excitation signal for ISO Class C profile.

For the optimization design of the active suspension system, the control input distribution matrix was defined as $\mathbf{B} = \begin{bmatrix} 1 & 1 \\ 0 & -2 \end{bmatrix}$, and the auxiliary mass correction matrix was

set to $\Delta\mathbf{M} = \mathrm{diag}(0.5, 0)$. The constraint thresholds were defined as $c_1 = 0.0115$ (RMS of body displacement) and $c_2 = 0.45$ (RMS of body acceleration). Using the SQP algorithm, the optimal design variables satisfying these constraints were obtained, as summarized in Table 4.

Table 4. Optimized design variables.

Category	Variable	Value
Eigenvalues (Y)	$\lambda_{3,4}$	-1.9450 ± 7.7588i
	$\mu_{1,2}$	-18.7191 ± 66.4209i
Predefined Vectors (X)	$\boldsymbol{w}_1, \boldsymbol{w}_2$	$-0.0104/0.7042$
	$\boldsymbol{w}_3, \boldsymbol{w}_4$	$0.8754/0.0933$

The gain matrices of the controller were obtained as

$$\mathbf{F} = \begin{bmatrix} 152.00 & -371.53 \\ 82.24 & -66.99 \end{bmatrix}, \ \mathbf{G} = \begin{bmatrix} -647.00 & -9509.00 \\ 3280.00 & -17244 \end{bmatrix}$$

The optimization objective function is defined as

$$J(\mathbf{F}, \mathbf{G}) = \sqrt{\|\mathbf{F}\|_F^2 + \|\mathbf{G}\|_F^2}$$

where $J(\mathbf{F}, \mathbf{G})$ measures the overall magnitude of the feedback gains and $\|\cdot\|_F$ denotes the Frobenius norm of a matrix.

Figure 4 illustrates the convergence process of the objective function during the dynamic response optimization. The objective value decreases rapidly at the initial stage and gradually stabilizes after approximately 20 iterations. The optimal solution is reached at the 40th iteration, with the corresponding minimum objective value of 1700.6571.

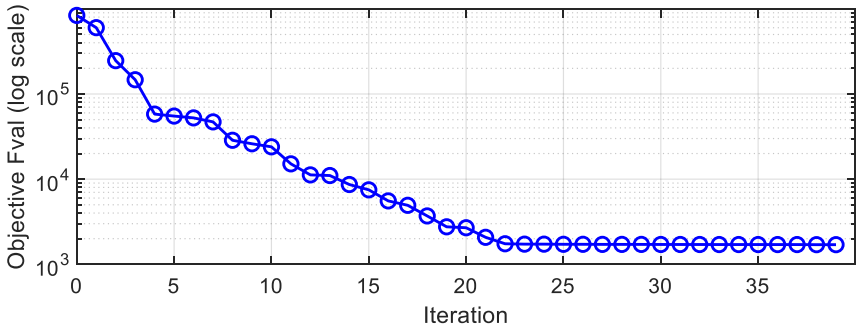


Figure 4. Convergence curve of the objective function in dynamic response optimization.

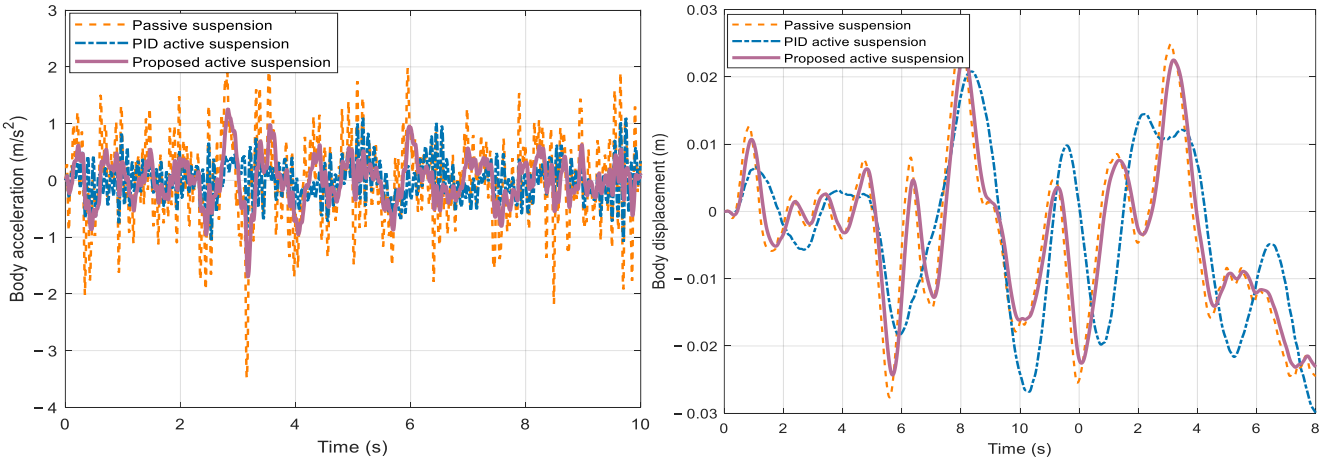
The dynamic equation of the closed-loop system can thus be expressed as

$$\mathbf{M}\ddot{\mathrm{x}} + \mathbf{C}\dot{\mathrm{x}} + \mathbf{K}\mathrm{x} - \mathbf{B}\mathbf{F}^T\dot{\mathrm{x}} - \mathbf{B}\mathbf{G}^T\mathrm{x} = 0$$

By substituting the obtained controller gain matrices $\mathbf{F}$ and $\mathbf{G}$ into the closed-loop dynamic equations, the time-domain responses of the system under a typical ISO Class C road excitation were obtained, as illustrated in Figure 5.

Figure 5a,b show the dynamic acceleration and displacement responses of three suspension systems: passive suspension, PID active suspension, and the proposed active suspension system. As seen in Figure 5a, the body acceleration response of the passive suspension (orange dashed line) exhibits larger fluctuations compared to both the PID active suspension (blue dash-dot line) and the proposed active suspension (purple solid

line). This indicates that the passive suspension struggles to maintain ride comfort under dynamic loading, as it is less effective at damping high-frequency oscillations.



(**a**) (**b**)

Figure 5. Comparison of responses between passive, PID active, and proposed active suspension systems: (**a**) Body acceleration response and (**b**) Body displacement response.

In contrast, both the PID active suspension and the proposed active suspension show significant improvement in damping, as evidenced by the smoother body acceleration waveforms in Figure 5a. The proposed active suspension, represented by the purple line, provides better vibration isolation than the PID active suspension. This is evident in the smaller amplitude and reduced peak acceleration, particularly during high-intensity input conditions (around time 2 s to 3 s and 7 s to 8 s). The PID system (blue dashed line) also performs better than the passive suspension but does not match the performance of the proposed system, particularly in terms of maintaining a stable response during transient disturbances.

For the body displacement response shown in Figure 5b, the same trend is observed. The passive suspension shows larger displacements, which indicates the system's inability to suppress body motion effectively. Both the PID and proposed active suspension systems, however, significantly reduce body displacement. The proposed system (purple line) again shows the least displacement compared to the PID system (blue dashed line), confirming its superior performance in controlling body motion. The proposed active suspension demonstrates smoother transitions and better suppression of displacement oscillations, further confirming its overall superior performance.

Table 5 presents the quantitative comparison of key performance metrics for the three suspension systems.

Table 5. Comparison of performance metrics between passive, PID active, and proposed active suspension systems.

Performance Metric	Passive Suspension	PID Active Suspension	Proposed Active Suspension
Peak body acceleration (m/s^2)	3.4771	1.0589	1.6990
RMS of body acceleration	0.7358	0.4459	0.4003
Peak body displacement (m)	0.02568	0.02415	0.02359
RMS of body displacement	0.01240	0.01246	0.01143
RMS of suspension deflection	0.00591	0.00939	0.00605

The proposed active suspension system achieves remarkable improvements in both body acceleration and displacement responses. Specifically, the maximum body accel-

eration decreases from 3.48 m/s^2 (passive suspension) to 1.70 m/s^2 (proposed active suspension), and the RMS of body acceleration is reduced from 0.7358 to 0.4003, corresponding to improvements of 51.1% and 45.6%, respectively. Compared to the PID active suspension, the proposed active suspension performs better, with a 6.5% improvement in RMS acceleration (from 0.4459 to 0.4003). This indicates that the proposed system provides superior vibration isolation and reduced discomfort for passengers. As shown in Table 6, this RMS range corresponds to the transition from "Fairly uncomfortable" to "Slightly uncomfortable," demonstrating a notable improvement in ride comfort.

Table 6. Relationship between weighted RMS acceleration and subjective ride comfort.

Weighted RMS Acceleration	Perceived Comfort Level
<0.315	Not uncomfortable
0.315∼0.63	Slightly uncomfortable
0.5∼1.0	Fairly uncomfortable
0.8∼1.6	Uncomfortable
1.25∼2.5	Very uncomfortable

In terms of body displacement, the proposed active suspension also shows superior performance. The maximum body displacement and RMS of body displacement are reduced by 8.1% and 7.9%, respectively, compared to the passive suspension. When compared to the PID active suspension, the proposed system shows a slightly better control performance, with a 7.9% reduction in RMS displacement. The proposed active suspension system performs slightly better in terms of dynamic deflection RMS compared to the passive suspension and PID active suspension, with a modest improvement of 6.05%. However, the primary performance improvements are seen in body acceleration and displacement, which are more closely related to ride comfort and system stability.

In summary, the proposed active suspension control method significantly improves system dynamics through the integration of eigenstructure assignment and dynamic response optimization. Compared to both passive suspension and alternative methods, the active system outperforms in key metrics such as body acceleration and displacement, leading to reduced vibration and enhanced ride comfort. These results demonstrate the effectiveness of the proposed control strategy.

5. Robustness Analysis

Although the controller design method employed in this study can effectively avoid modeling-related errors, it may still be influenced by system uncertainties or inaccurate fitting of the frequency response functions, which can distort the resulting eigenstructure assignment of the system. In this section, the robustness of the proposed method is assessed using the numerical example presented in Section 4. Analogous to the numerical example, the first pair of system eigenvalues is assigned to $\mu_{1,2} = -18.7191 \pm 66.4209i$, while the second pair is kept unchanged at $\mu_{3,4} = -1.9450 \pm 7.7588i$. The control matrix $\mathbf{B}$ is also defined to be identical to that used in the example.

Consider the 2-DoF quarter-car suspension system used in the numerical example. To emulate possible measurement noise or identification errors, the receptance matrix obtained from simulation is artificially perturbed at one or two selected entries. The contaminated receptance is defined as

$$\hat{h}_{i,j}(\mu_k) = h_{i,j}(\mu_k)\, rand(0.95,\ 1.05)$$

where $\hat{h}_{i,j}(\mu_k)$ denotes the perturbed receptance, $h_{i,j}(\mu_k)$ is the nominal (true) receptance, and $rand(0.95, 1.05)$ is a uniformly distributed random number between 0.95 and 1.05, corresponding to at most a 5% deviation from the nominal value.

Figure 6a,b, respectively, present the results of 1000 Monte-Carlo simulations. The four rectangles represent the regions of the obtained eigenvalues and are defined as follows:

$$\text{Region}(\mu_k) = \mu_k + [-0.05, 0.05] \pm [-0.05, 0.05]i$$

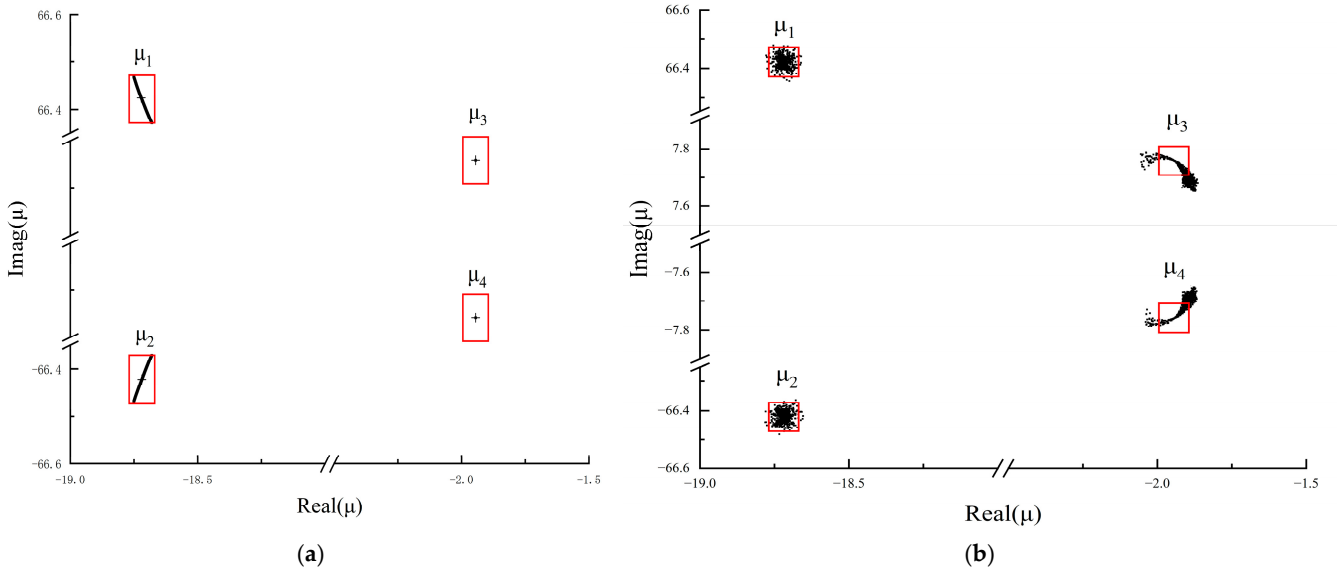


Figure 6. Eigenvalue spread with contaminated receptance matrices, where (**a**) shows the case with one contaminated element and (**b**) illustrates the case with two contaminated elements.

From Figure 6a it can be seen that all obtained eigenvalues fall within small regions close to the nominal values of the targeted eigenvalues. Because more contaminated elements are included in Figure 6b larger variations in the imaginary parts are observed. Nevertheless, the vast majority of the eigenvalues still cluster within relatively small regions. Therefore, the proposed method can be regarded as robust with respect to errors in the measured receptance (frequency response) matrix of the example system.

6. Conclusions

This study has proposed an eigenstructure-oriented optimization method for active suspension control, integrating eigenstructure assignment with dynamic response optimization. By redistributing the system eigenstructure, the method suppresses vibrations and improves ride comfort. In a quarter-car case study, the proposed controller reduces peak body acceleration by 51.1% and RMS acceleration by 45.6% and yields comparable reductions in body displacement. Compared with passive suspension and PID active suspension, it achieves superior performance in key indices such as body acceleration and displacement, resulting in noticeably improved ride comfort. Robustness studies further show that the method remains effective under 5% perturbations in the receptance matrix of a 2-DoF damped system, indicating good tolerance to data inaccuracies with only minor impact on overall system performance.

Despite these advantages, the method is subject to two main applicability constraints. First, although the formulation in principle requires only partial system information for eigenstructure assignment, in practice it is difficult to obtain full-vehicle receptance data with sufficient spatial coverage and accuracy, which may reduce the achievable performance. Second, the required number of input channels is determined by the total number

of assigned and preserved eigenvalues together with the system degrees of freedom; this requirement often conflicts with packaging, space and cost constraints in production vehicles and thus limits the method's direct engineering deployment.

Future work will therefore proceed along two directions. The first is to extend the eigenstructure-oriented optimization method from the quarter-car model to full-vehicle modeling and control, so as to capture the coupled dynamics of the entire vehicle over a wider range of road profiles and operating conditions. On this basis, strategies for reducing the number of actuators while preserving acceptable control performance will be explored and validated via multi-domain co-simulation, thereby narrowing the gap between numerical studies and real-vehicle operation. The second direction is to further investigate the intrinsic relationship between eigenstructure and time-domain responses, with the goal of relaxing the dependence on detailed receptance data. Machine-learning-based surrogate models for large-scale systems will be developed to enhance the adaptability and computational efficiency of the eigenstructure-oriented active suspension framework.

Author Contributions: Conceptualization, H.M.; methodology, Y.D.; software, Y.D.; validation, Y.D.; writing—original draft preparation, Y.D.; writing—review and editing. All authors have read and agreed to the published version of the manuscript.

Funding: This research was funded by the Provincial Natural Science Foundation of Shanxi Province, China, grant number 202303021221108.

Data Availability Statement: The data is available on request to the first author.

Acknowledgments: We are deeply grateful for the constructive feedback provided by the anonymous reviewers.

Conflicts of Interest: The authors declare no conflicts of interest.

References

1. Dandavate, K.D. A Review on Controlling Methods for Active Suspension Systems. *Int. J. Res. Appl. Sci. Eng. Technol.* **2023**, *11*, 1675–1680. [CrossRef]
2. Goga, V.; Kľúčik, M. Optimization of Vehicle Suspension Parameters with Use of Evolutionary Computation. *Procedia Eng.* **2012**, *48*, 174–179. [CrossRef]
3. Ding, F.; Wang, B.; Liu, M. Research on LQR Control of Vehicle Active Suspension. *Mach. Des. Res.* **2020**, *36*, 52–55.
4. Zhao, Z.; Wang, C.; Zhao, J.; Du, W. LQR Force Command Planning Based Sliding Mode Control for Active Suspension System. *J. Syst. Control Eng.* **2024**, *238*, 373–385. [CrossRef]
5. Abut, T.; Salkim, E. Control of Quarter-Car Active Suspension System Based on Optimized Fuzzy Linear Quadratic Regulator Control Method. *Appl. Sci.* **2023**, *13*, 8802. [CrossRef]
6. Başak, H. Hybrid Coati–Grey Wolf Optimization with Application to Tuning Linear Quadratic Regulator Controller of Active Suspension Systems. *Eng. Sci. Technol. Int. J.* **2024**, *56*, 101765. [CrossRef]
7. Parvez, Y.; Chauhan, N.R.; Srivastava, M. Vibration Control and Comparative Analysis of Passive and Active Suspension Systems Using PID Controller with Particle Swarm Optimization. *J. Inst. Eng. India Ser. C* **2025**, *106*, 1–19. [CrossRef]
8. Abut, T.; Salkim, E.; Demosthenous, A. Performance Improvement in a Vehicle Suspension System with FLQG and LQG Control Methods. *Actuators* **2025**, *14*, 137. [CrossRef]
9. Li, J.; Jia, C.; Cheng, L.; Zhao, Q. Constrained State Feedback H∞ Control of Active Suspension System for In-Wheel Motor Electric Vehicles. *J. Jilin Univ. Eng. Technol.* **2021**, *53*, 1521–1529.
10. Wu, X.; Zhou, L.; Zhang, M.; Jiang, H.; Liu, W.; Hu, J. Sliding Mode Adaptive Control of Active Suspension System Combined with Particle Filter State Observation. *J. Hunan Univ. Nat. Sci.* **2024**, *51*, 19–27.
11. Hu, Y.; Peng, J. Adaptive Fault-Tolerant Control of Active Suspension Systems Considering Input and Output Constraints. *Control Decis.* **2025**, *40*, 693–698.
12. Lyu, B.; Zhang, R. Semi-Active Air Suspension System Based on Fuzzy PID Control. *Mach. Des. Manuf.* **2025**, *5*, 79–84.
13. Chantranuwathana, S.; Peng, H. Adaptive Robust Force Control for Vehicle Active Suspensions. *Int. J. Adapt. Control Signal Process.* **2004**, *18*, 83–102. [CrossRef]

14. Qi, X.; Liu, W.; Yang, Y.; Lu, J. Adaptive Finite-Time Fuzzy Control for Nonlinear Systems with Input Quantization and Unknown Time Delays. *J. Frankl. Inst.* **2020**, *357*, 7718–7742. [CrossRef]
15. Sun, W.; Gao, H.; Yao, B. Adaptive Robust Vibration Control of Full-Car Active Suspensions with Electrohydraulic Actuators. *IEEE Trans. Control Syst. Technol.* **2013**, *21*, 2417–2422. [CrossRef]
16. Min, X.; Li, Y.; Tong, S. Adaptive Fuzzy Output Feedback Inverse Optimal Control for Vehicle Active Suspension Systems. *Neurocomputing* **2020**, *403*, 257–267. [CrossRef]
17. Dong, X.; Zhao, D.; Yang, B.; Han, C. Fractional-Order Control of Active Suspension Actuator Based on Parallel Adaptive Clonal Selection Algorithm. *J. Mech. Sci. Technol.* **2016**, *30*, 2769–2781. [CrossRef]
18. Piao, C.; Liu, X.; Lu, C. Lateral Control Using Parameter Self-Tuning LQR on Autonomous Vehicle. In Proceedings of the 2019 International Conference on Intelligent Computing, Automation and Systems (ICICAS), Chongqing, China, 6–8 December 2019; IEEE: Piscataway, NJ, USA, 2019; pp. 913–917.
19. Li, Q.; Chen, Z.; Song, H.; Dong, Y. Model Predictive Control for Speed-Dependent Active Suspension System with Road Preview Information. *Sensors* **2024**, *24*, 2255. [CrossRef]
20. Tang, H.H.; Ahmad, N.S. Enhanced Fuzzy Logic Control for Active Suspension Systems via Hybrid Water Wave and Particle Swarm Optimization. *Int. J. Control Autom. Syst.* **2025**, *23*, 560–571. [CrossRef]
21. Wang, T.; Zhang, H.; Sui, S. Observer-Based Adaptive Neural Network Event-Triggered Quantized Control for Active Suspensions with Actuator Saturation. *Neurocomputing* **2025**, *614*, 128770. [CrossRef]
22. Li, Y.; Wang, T.; Liu, W.; Tong, S. Neural Network Adaptive Output-Feedback Optimal Control for Active Suspension Systems. *IEEE Trans. Syst. Man Cybern. Syst.* **2021**, *51*, 4021–4032. [CrossRef]
23. Wang, C.; Cui, X.; Zhao, S.; Zhou, X.; Song, Y.; Wang, Y.; Guo, K. A Deep Reinforcement Learning-Based Active Suspension Control Algorithm Considering Deterministic Experience Tracing for Autonomous Vehicle. *Appl. Soft Comput.* **2024**, *153*, 111259. [CrossRef]
24. Gao, X.; Du, Y.; Han, S.; Zhao, W.; Zhou, J.; Zhang, T.; Chen, C.L.P. Multi-Agent Reinforcement Learning for Vibration Control of Regenerative Active Suspension. *Eng. Appl. Artif. Intell.* **2025**, *153*, 110809. [CrossRef]
25. Abut, T.; Salkim, E.; Tugal, H. Active Suspension Control for Improved Ride Comfort and Vehicle Performance Using HHO-Based Type-I and Type-II Fuzzy Logic. *Biomimetics* **2025**, *10*, 673. [CrossRef] [PubMed]
26. Mottershead, J.E.; Friswell, M.I. Model Updating in Structural Dynamics: A Survey. *J. Sound Vib.* **1993**, *167*, 347–375. [CrossRef]
27. Belotti, R.; Richiedei, D. Dynamic Structural Modification of Vibrating Systems Oriented to Eigenstructure Assignment through Active Control: A Concurrent Approach. *J. Sound Vib.* **2018**, *422*, 358–372. [CrossRef]
28. Ram, Y.M.; Mottershead, J.E. Multiple-Input Active Vibration Control by Partial Pole Placement Using the Method of Receptances. *Mech. Syst. Signal Process.* **2013**, *40*, 727–735. [CrossRef]
29. Richiedei, D.; Tamellin, I.; Trevisani, A. Pole–Zero Assignment by the Receptance Method: Multi-Input Active Vibration Control. *Mech. Syst. Signal Process.* **2022**, *172*, 109108. [CrossRef]
30. Adamson, L.J.; Fichera, S.; Mottershead, J.E. Receptance-Based Robust Eigenstructure Assignment. *Mech. Syst. Signal Process.* **2020**, *140*, 106666. [CrossRef]
31. Ariyatanapol, R.; Xiong, Y.P.; Ouyang, H. Partial Pole Assignment with Time Delays for Asymmetric Systems. *Acta Mech.* **2018**, *229*, 2619–2629. [CrossRef]
32. Zhang, S.; Ouyang, H. Receptance-Based Partial Eigenstructure Assignment by State Feedback Control. *Mech. Syst. Signal Process.* **2022**, *168*, 108682. [CrossRef]
33. Richiedei, D.; Tamellin, I.; Trevisani, A. Unit-Rank Output Feedback Control for Antiresonance Assignment in Lightweight Systems. *Mech. Syst. Signal Process.* **2022**, *164*, 108286. [CrossRef]
34. *ISO 8608:2016*; Mechanical Vibration. Road Surface Profiles. Reporting of Measured Data. ISO: Geneva, Switzerland, 2016. Available online: https://cdn.standards.iteh.ai/samples/71202/05b2151f255b44928f80acb897fc0c2c/ISO-8608-2016.pdf (accessed on 5 November 2025).

Disclaimer/Publisher's Note: The statements, opinions and data contained in all publications are solely those of the individual author(s) and contributor(s) and not of MDPI and/or the editor(s). MDPI and/or the editor(s) disclaim responsibility for any injury to people or property resulting from any ideas, methods, instructions or products referred to in the content.